#09

MODEL STUDIES OF JOINTED-ROCK BEHAVIOR

by

H.H. Einstein, Research Associate, M.I.T.
R.A. Nelson, Civil Engineer, U.S. Army Corps of Engineers
R.W. Bruhn, Civil Engineer, U.S. Army Corps of Engineers
R.C. Hirschfeld, Associate Professor of Civil Engineering, M.I.T.

Preprint of a paper prepared for the

Eleventh Symposium on Rock Mechanics

Berkeley, California

June 16-18, 1969

69-39
DND

LIBRARY COPY
Materials & Research Dept.

ClibPDF - www.fastio.com

Table of Contents

Page No.

A. Introduction 1

B. Procedure. 2

1. Selection of Model Material. 2
   a. Selection Criteria 2
      (1) Similitude requirements. 2
      (2) Practical testing limitations. 5
   b. Selection Procedure. 5
   c. Characteristics of the Model Material. 6
   d. Preparation of Model Material. 7

2. Model Configuration. 8

3. Triaxial Testing Equipment 8

4. Testing Procedure. 9

C. Results. 10

1. Intact Material. 10

2. Sliding Along a Single Plane 11
   a. Direct Shear Tests 11
   b. Triaxial Tests 12

3. Sliding and Fracture at High Normal Stress 13

4. The Influence of Multiple Joints 14

5. Failure Surfaces 17

D. Conclusions. 19

Acknowledgements 21

Bibliography 22

ClibPDF - www.fastio.com

MODEL STUDIES OF JOINTED ROCK BEHAVIOR

A. Introduction

The objective of the model studies described in this paper is to determine the effect of planar discontinuities on the strength and deformability of a rock mass. A model material was used because it satisfied concurrently three requirements that available natural-rock samples did not: (1) low strength, which was desirable for minimizing the loads that had to be applied in the laboratory; (2) ease of producing test specimens with geometrically regular joint patterns; (3) uniformity of the test specimens.

The model tests were performed on specimens made from a single modeling material and tested under triaxial stress conditions with $\sigma_2 = \sigma_3$. Results are presented in this paper for tests on specimens that had (1) a single joint set inclined at several angles to the major principal direction, including 0° and 90°, and (2) two joint sets that were mutually perpendicular, one set perpendicular to and one set parallel to the major principal direction. Several different joint spacings were used in each series. Future tests are planned to include a series with two sets of joints that make several angles with each other and with the major principal direction.

The results of model tests and tests on cores of jointed rock by several investigators (e.g. Müller and Pacher (14)*,

* Numbers in parantheses refer to corresponding items in the bibliography.

ClibPDF - www.fastio.com

Moore (13), Krsmanovic and Milic (9), Hayashi (6), Rosenblad (20), Jaeger (8), Lane and Heck (10)) have contributed significantly to the design of these experiments, which are believed to be the first in which a comprehensive study has been made of the combined effects under triaxial loading of joint spacing and joint orientation (Fig. 1).

B. Procedure

1. Selection of Model Material

A substantial investigation was made to select an appropriate modeling material. That investigation has been described in detail by Nelson and Hirschfeld (15), and the most important aspects of it are reviewed in the following paragraphs.

a. Selection Criteria

(1) Similitude requirements

The strength and deformability of a jointed rock mass can be represented by the function

$$s = f\ (\sigma_c,\ \sigma_t,\ \sigma_{conf},\ \Phi_j,\ \Phi_i,\ E,\ \nu,\ \rho,\ D,\ \alpha,\ \varepsilon,\ g,\ \dot{\varepsilon})$$

where s = strength

σ_c = unconfined compressive strength

σ_t = unconfined tensile strength

σ_{conf} = confining stress

Φ_j = joint surface friction angle

Φ_i = angle of internal friction of intact material, this angle may vary (curved Mohr envelope) and thus several Φ_i may have to be used.

ClibPDF - www.fastio.com

E = modulus of deformation of intact material

ν = Poisson's ratio

ρ = mass density

D = joint spacing

α = angle between joint plane and major principal direction

ε = strain

g = acceleration of gravity

$\dot{\varepsilon}$ = strain rate

This function can be written in terms of dimensionless factors expressed in terms of the above variables, for example:

$$s/\rho gD = f\left(\frac{\sigma_c}{\rho gD}, \frac{\sigma_t}{\rho gD}, \frac{\sigma_{conf}}{\rho gD}, \Phi_j, \Phi_i, \frac{E}{\sigma_c}, \nu, \dot{\varepsilon}\sqrt{\frac{D}{g}}, \varepsilon, \alpha\right)$$

Each of the dimensionless factors (π factors) must be the same for model and prototype ($\pi_{model} = \pi_{prototype}$) if the model is to fulfill the requirements of similitude. It was not the purpose of this study to model any particular prototype rock but rather to ensure that the model corresponded to the general range of <u>brittle</u> rocks that are most commonly encountered in civil engineering.

The first two π-factors ($\frac{\sigma_c}{\rho gD}$ and $\frac{\sigma_t}{\rho gD}$) were combined into a single π-factor ($\frac{\sigma_c}{\sigma_t}$), which, together with the shape of the stress-strain curve, the modulus of deformation, and the failure mode, is an indicator of "brittleness". Typical values of ($\frac{\sigma_c}{\sigma_t}$) for brittle rocks are between 10 and 20, occasionally even higher. Values that are higher than 20 are generally the product of investigations

ClibPDF - www.fastio.com

in which the tensile strength was determined by means of point-load tests, which tend to give lower values than carefully conducted tension tests, and correspondingly higher apparent values for the ratio $(\frac{\sigma_c}{\sigma_t})$. Values that approach 10, which was used as the prototype value for this investigation, have been determined by Brace (2) by extrapolating from the results of very carefully conducted triaxial extension tests on quartzite, granite, and diabase, and by Bieniawski (1).

The shape of the stress-strain curve, as a measure of "brittleness", cannot be simply expressed in terms of a numerical parameter. For this investigation, the qualitative requirement was arbitrarily established that the intact model material should have an approximately linear stress-strain curve up to failure, for confining stresses up to about 1500 psi. The modulus of elasticity E was included in the π-factor $(\frac{E}{\sigma_c})$.

Several of the variables that enter into the π-factors cannot be varied over more than a narrow range and these include Φ_j, Φ_i, ν, ρ, and g. The remaining variables, σ_{conf}, D, and $\dot{\varepsilon}$ are limited primarily by practical testing constraints, as described below.

Within the above limitations, it is impossible to satisfy all of the similitude requirements with a single modeling material. The π-factors that could practically be varied and that were considered most critical were $(\frac{\sigma_c}{\sigma_t})$ and $(\frac{E}{\sigma_c})$.

ClibPDF - www.fastio.com

There is a so-called "size effect" that is not taken into consideration by the dimensional analysis: The larger the volume of material tested, the lower the strength. A special series of tests is now underway to evaluate the significance of the size effect.

(2) Practical testing limitations

The compressive strength of the modeling material is limited by the maximum load that can be applied with the available testing equipment, and the strain rate that can be used for the model tests will also be limited to the practical range for the available testing equipment.

The modeling material should obviously be one that can be readily cast into any desired shape without shrinkage or distortion during curing. It should also be uniform within a single specimen and reproducible from test to test.

The joint spacing in the model cannot be less than about 1/2 inch because of the difficulty of casting and handling smaller pieces.

b. Selection Procedure

A literature review on model materials (see Nelson and Hirschfeld(15)) narrowed the choice to gypsum plaster, mixed with water and admixtures. A total of 22 different mixes were tested. The gypsum types used were Hydrocal B-11, Ultracal 60, and White Molding Plaster. The admixtures used were Celite (diatomaceous earth), Kaolinite and sand.

ClibPDF - www.fastio.com

Observations of bleeding, shrinkage, surface characteristics, and number and size of air-bubble holes were made after casting and curing. The uniaxial compressive strength was measured on cylindrical samples (d = 2", h = 4") and the uniaxial tensile strength was measured on dogbone-shaped samples. In Fig. 2 several stress-strain curves of different gypsum mixes are presented.

The best combination of brittle behavior, acceptable strength, lack of bleeding, smooth surface characteristics, and minimum number of bubble holes was found for Hydrocal B-11 with a $\frac{\text{Water}}{\text{Hydrocal}}$ ratio of 0.45 (by weight) and a $\frac{\text{Water}}{\text{Celite}}$ ratio of 32 (by weight).

Uniaxial compression and tension tests were used as control tests during the course of the model study. Control tests were performed at regular intervals and whenever a new bag of Hydrocal was used.

c. Characteristics of the Model Material Selected

The most important material properties and π-factors of the model material and its equivalent prototype are listed in Table 1. Table 1 also contains the corresponding values of some rocks (granite and quartzite values taken from Brace (2) and Bieniawski (1)). As can be seen in Table 1 there is some difference between the π-factors for the model material and for the particular rock types used in the comparison. However, the values for the model material seem to be in a reasonable range

ClibPDF - www.fastio.com

for an approximate representation of rock. As will be seen in the course of this paper the mechanical characteristics (stress-strain curves, Mohr envelopes) compare well with the characteristics of granite as found by Byerlee (4).

d. Preparation of Model Material

The preparation, i.e., mixing and curing of the samples must be carefully controlled to obtain reproducible material properties. Raphael (19) presents a thorough discussion of this problem. The gypsum, water, and celite were mixed for six minutes, a duration of mixing that led to practically no bleeding. Then the mix was poured into the mold which was placed on a vibrating table and vibrated for one minute. This vibration results in the expulsion of much of the air without causing segregation of the mix components.

The most critical part of the preparation is proper curing of the samples. Hydrated gypsum has a water content of 18.6% at which no water remains in the structure except the water that is chemically bound. If more water is driven off the hydrated gypsum is changed into hemihydrates or anhydrite. Gypsum at a water content of 18.6% has a higher strength than gypsums at greater or lesser water contents. All the different-sized model samples were cured at a temperature of 105°F. until they reached the optimum water content of 18.6%, which took between 2 and 20 days, depending on sample size.

ClibPDF - www.fastio.com

2. Model Configuration

The model specimen is a 2" x 4" x 8" prism. The mold, which consists of stainless steel blocks and plates which is shown in Figs. 3 and 4, can be used to cast model specimens having different joint spacings and inclinations. A slightly different mold with a single "joint plate" was used for prisms containing a single joint. Some of the possible model configurations that can be produced with the mold are shown in Fig. 7.

3. Triaxial Testing Equipment

Fig. 5 is a schematic of the triaxial equipment. The principal parts are a cylindrical triaxial cell designed for a hydrostatic cell pressure of 2000 psi and a hydraulic 200,000 pound loading machine for the application of the axial load. The triaxial cell is filled with a nonconductive cell fluid (dimethyl silicone oil) and cell pressure is maintained by a tank filled with nitrogen under pressure. The main parts of the cell are shown in Fig. 6. Axial load was applied to the sample by means of a piston, a ball and a prismatic steel top cap. The pedestal contains holes to provide for pore pressure measurements (although no pore pressure measurements have been made so far). A double membrane covers the sample: an inner 1/32" neoprene sheet provides protection against puncturing of an external 1/1000" membrane. The external membrane is sealed to the cap and pedestal by special elliptical clamps.

ClibPDF - www.fastio.com

The pedestal is equipped with two sets of four SR4 strain gauges in series so that the axial load on the specimen can be measured inside the cell, thus eliminating errors due to piston friction which is significant in tests with inclined joints. The strain gauges are covered with a layer of epoxy resin, they are inside the membrane, and a nonconductive cell fluid is used to provide protection against short circuiting.

The axial displacements were measured with a direct-current differential transformer (DCDT) connected to the piston and the cell. A calibration curve was determined to correct for the deformation of the apparatus itself.

The axial load and the axial displacement were continuously recorded and plotted by an X-Y recorder.

4. Testing Procedure

The sequence of experiments proceeded from rather simple cases with few variables to cases with many variables, as shown in Fig. 7.

(a) Intact samples

(b) Samples with a single joint at various inclinations to the major principal direction.

(c) Samples with a single set of joints, at various spacings, parallel to the major principal direction.

(d) Samples with a single set of joints, at various spacings, perpendicular to the major principal direction.

(e) Samples with two orthogonal sets of joints, at various spacings, one set perpendicular to and one set parallel to the major principal direction.

(f) Samples with one set of joints, at various spacings, at various angles to the major principal direction. (Tests now in progress; no results reported in this paper.)

ClibPDF - www.fastio.com

Each series of tests consisted of several tests at different confining stresses. Unconfined compression tests and triaxial tests at 500, 1000 and 1500 psi confining stress were usually performed, but in some of the experiments intermediate values were chosen, and for intact samples confining stresses as high as 2000 psi were applied.

C. Results

1. Intact Material

The model material behaves in an essentially brittle manner at confining stresses less than 1500 psi; the ascending portion of the stress-strain curve is very nearly a straight line and after failure a relatively sharp decrease in stress occurs, as can be seen in Fig. 8. At confining stresses above 1500 psi the ascending portion is curved and the stress drop after failure becomes less pronounced. At 2000 psi confining stress the behavior is definitely ductile: there is no stress drop after reaching the maximum stress and the ascending portion of the stress-strain curve is strongly concave downward near failure.

The deformability of the model material is thus stress dependent, similar to some natural rocks, as observed by Byerlee (5).

Not only the stress-strain behavior but also the failure mode is affected by the confining stress. Plumose (brittle) structures develop in the failure zone at low confining stress,

ClibPDF - www.fastio.com

and multiple failure planes and plastic flow develop at high confining stress. These phenomena, which again correspond to the behavior of most natural rocks, will be discussed in more detail in Sections C.3 and C.5. Stick-slip behavior which is common to many natural rocks has also been observed in these experiments on the intact model material.

Increasing confining stress also affects the strength of the intact material as can be seen in the Mohr diagram of Fig. 9. The Mohr failure envelope is significantly curved, as it is for many rocks.

The qualitatively similar behavior of natural rock and the model material implies that the modeling material selected is a reasonable one.

2. Sliding Along a Single Plane

a. Direct Shear Tests

The direct shear tests were performed in the apparatus shown schematically in Fig. 10. A gypsum block 1" x 1/2" x 1/2" was slid over a block 2" x 1/2" x 1/2". Normal load was applied by means of dead weights and the shear force by a screw drive moving at a constant rate of 0.007"/min. Shear force and displacement were continuously recorded by a load cell and a direct-current differential transformer(DCDT).

The Mohr envelope for the direct shear tests (see Fig. 11) is a straight line inclined at 39° up to a normal stress of about 1000 psi; between 1000 psi and 1500 psi it is concave

ClibPDF - www.fastio.com

downward; above 1500 psi it is approximately a straight line inclined at 33°, up to 2000 psi, the maximum stress at which direct shear tests could be performed in this apparatus. The sliding behavior at normal stresses greater than 2000 psi was determined in triaxial tests.

b. Triaxial Tests

Two failure modes are possible (depending on joint inclination and confining stress) if a jointed sample is tested under triaxial conditions: (1) sliding along the joint (or joints); or (2) failure through the intact material. Nelson and Hirschfeld (15) show how the limiting conditions for the two failure modes can be graphically presented.

In this section only sliding failure will be discussed. Sliding failure occurs if a single joint in the triaxial specimen is inclined at e.g. 30° or 45° to the major principal direction. The range of normal stresses for which data have been obtained is between 1000 and 4000 psi. The Mohr envelope (Fig. 12) is basically a straight line except for stresses in the range 0 - 1500 psi where it coincides with the partially curved envelope of the direct shear tests.

The initially curved sliding envelope (sometimes simplified as an intercept on the τ-axis) is a feature that is common to some natural rocks as has been shown, for example, by Byerlee (5). It can be explained by the effect of dilatancy at low stresses, i.e. the riding-up over surface asperities at low stresses as

ClibPDF - www.fastio.com

shown by Patton (18).

It is of interest to compare the Mohr envelope for sliding along a pre-existing joint with the Mohr envelope for "residual sliding", i.e. sliding along a failure surface after fracture has taken place in an originally intact sample. The residual-sliding envelope (Fig. 12) has the same inclination as the envelope for sliding along a pre-existing joint but the shear stress values are greater. In other words, the apparent intercept on the τ-axis is greater. The failure surface of the intact sample is considerably rougher than the surfaces of the pre-existing joints. The greater roughness apparently increases the dilatancy and thus shifts the Mohr envelope upward (Patton (18)).

3. Sliding and Fracture at High Normal Stress

As can be seen in Fig. 13 the Mohr failure envelope for intact material and the envelope for sliding along a joint in the same material intersect or converge at a normal stress of about 4500 psi. The results of experiments with samples containing a single joint inclined at 45° make it possible to describe what happens physically in this transition range. The samples fail by sliding along the pre-existing joint at confining stresses up to 1500 psi. However, at a confining stress of 1500 psi or greater failure takes place primarily by fracture through the intact material and sliding along the pre-existing joint is only of secondary importance. The confining stress of approximately

ClibPDF - www.fastio.com

1500 psi corresponds to a normal stress of about 4500 psi on the failure plane, which is the stress at which the two failure envelopes converge. This transition from sliding behavior to fracture as postulated by Orowan (16) has been supported by experiments on rocks by other authors (Byerlee (5), Maurer (12)). The transition from sliding to fracture coincides with the transition from brittle to ductile behavior that is apparent in the stress-strain curves in Fig. 8. The normal stresses on the joint plane become so large that the corresponding shear stresses are sufficient to cause failure through the intact material, and little or no sliding along the joint plane takes place. Sliding along freshly created fracture surfaces in this stress range is limited for the same reasons, and this explains the development of multiple failure surfaces in the ductile region. Thus, the number of failure surfaces increases with the confining stress. This can be seen by observing intact samples but is especially impressive in the horizontally jointed samples where the failure surfaces intersect the joint planes and can be examined after the test. The example in Fig. 14 shows that the number of failure surfaces is substantially greater for a confining stress of 1500 psi than for 500 psi.

4. The Influence of Multiple Joints

As has been mentioned in Section B.4. the results presented in this paper are restricted to joint sets parallel to or perpendicular to the principal directions. Thus, only failure across

ClibPDF - www.fastio.com

joints and through intact material will be treated, but not sliding along multiple joints. To simplify the description of the experiments the following expressions will be used:

Vertical Joints for joints in a joint set parallel to the major principal stress.

Horizontal Joints for joints in a joint set perpendicular to the major principal stress.

Orthogonal Joints for joints in two joint sets that are respectively parallel and perpendicular to the major principal direction.

These joint configurations are shown in Fig. 15. The joint spacings studied to date were: 1/2", 1", and 2" for the vertical and horizontal joints and 1/2" for the orthogonal joints. The influence of joint configuration on strength and deformability is very distinct and systematic.

The Mohr failure envelopes for different joint configurations have been plotted in Fig. 16 together with the failure envelope for intact material. The strength of the jointed model at a given normal stress is lowest for orthogonal joints, higher for horizontal joints, and highest for vertical joints. For each joint configuration there is a systematic strength increase with increasing joint spacing.

All of the failure envelopes of jointed material are lower than the envelope of intact material, despite the fact that failure occurs by fracture through the intact material and not by sliding along the joint surfaces. The envelopes converge into a single

ClibPDF - www.fastio.com

envelope and intersect the sliding envelope at a normal stress of about 3000 - 4000 psi, which correspond to confining stresses of about 900 and 1300 psi, as shown in Fig. 16. Since the number of tests is small no final statement concerning this convergence can be made.

The fact that the failure envelope of a jointed material is lower than that of intact material has also been observed by Rosengren and Jaeger (21). They used marble in which the grains were in their original locations and completely interlocked but were artificially separated along the grain boundaries by heat treatment. The failure envelope of their artificially "jointed" marble is about 2000 psi lower and parallel to the envelope of the untreated marble.

The joint configuration has a similar systematic effect on the deformability, as can be seen from the stress-strain curves in Figs. 17 and 18: A measure for the deformability is the stress at which the transition occurs from basically brittle behavior (with a substantial straight portion of the stress-strain curve and a sharp drop in the stress beyond the peak) to a basically ductile behavior (with a more curved stress-strain relation and continued plastic yielding at the peak stress). The confining stress at which this transition takes place is largest for intact material, smaller for vertically jointed material, still smaller for horizontally jointed material, and smallest for orthogonally jointed material. In addition, there is a systematic increase of this transition stress with increasing joint spacing for vertically

ClibPDF - www.fastio.com

and horizontally jointed samples (the spacing of the orthogonally jointed samples not having been varied as yet). The trend is more pronounced for horizontally jointed models than for those containing vertical joints because the deformability of the joints themselves has a greater influence if they are perpendicular to the major principal stress (which is the direction in which the strain is measured).

The initial flat portion of the stress-strain curve is probably the result of the closing of microcracks, the closing of the joints, and the seating of the loading apparatus. (The unconfined tests on orthogonally jointed samples show extremely high deformability and low strength, which is due to partial instability of the system).

5. Failure Surfaces

The inclination of the failure surfaces in intact material corresponds well to the value predicted by the Mohr theory. By contrast there is a considerable deviation from the predicted inclination in jointed samples, although the observed inclination does decrease with increasing confining stresses as would be expected for a Mohr failure envelope that is concave downward. In vertically jointed samples the failure surfaces are often non-planar.

Two physical features which have been observed on the failure surfaces of the models seem analogous to features in natural rock: plumose structure and slickensides.

ClibPDF - www.fastio.com

A plumose structure on the failure surface was evident in many of the samples that have been tested in uniaxial compression, all of which failed in a brittle manner. This type of structure has been related to crack propagation in brittle failure by McClintock (11) and Smekal (22), the latter giving experimental proof for the hypothesis. The observations made on these model specimens thus support the relationship between brittle fracturing and plumose structure.

Slickensides developed on the failure surfaces of model samples that have been tested at confining stresses of up to 1000 psi. At greater confining stresses no slickensides developed. The most interesting characteristics of the slickensides are steps that point in the "wrong direction", i.e. the steep side is opposed to the direction of sliding. As can be seen in Fig. 19 these steps are a part of secondary conjugate shear planes along which displacement occurs after the primary failure surface has been created. Steps in the direction opposed to the sliding movement have also been observed by Paterson (17) and Hoskins (7) in laboratory tests on natural rock. For field studies of the direction of displacement along faults, these observations make doubtful the assumption that the fault displacement is always in the direction of that feels "smooth" rather than in the direction that feels "rough".

An extensive description and investigation of the various characteristics of the failure surface and the failure mode has been given by Bruhn (3).

ClibPDF - www.fastio.com

D. Conclusions

The model material - a gypsum plaster consisting of Hydrocal B-11,Celite, and water - was selected by dimensional analysis and by qualitative indicators of brittle behavior that showed it to be similar to brittle rocks. Although the model material behaves in a brittle manner at low confining stresses, it becomes ductile at high confining stresses, a trend which is common for many rocks. In the range of normal stress in which the transition from brittle to ductile behavior of the intact material occurs, it was observed that jointed samples, which had failed by sliding along favorably inclined pre-existing joints at lower stresses, began to fail by fracture through the intact material, despite the presence of the pre-existing, favorably inclined joints. For similar reasons multiple failure surfaces are likely to form in samples that are sheared at high confining stresses whereas only one or two failure surfaces develop in samples sheared at low confining stresses. The observed ductile behavior is caused by this formation of multiple failure planes, plus actual palstic flow in the constituent crystals.

The strength and deformability of a model jointed-rock depend on: (1) confining stresses, (2) material properties, (3) joint properties, (4) joint inclination, (5) joint spacing. The results of this model study provide empirical data for making qualitative and quantitative correlations between these factors and the strength and deformability of a rock mass. The present model studies are being extended to other joint configurations and will

ClibPDF - www.fastio.com

make use of other intact materials.

The physical features that can be observed on the failure surfaces and the inclination of the failure surfaces give some insight into the failure mechanism. Brittle failure is characterized by plumose structures. Slickensides are present on failure surfaces of this gypsum modeling material when sheared at medium stresses, and the steep sides of the slickensides are opposed to the sliding direction.

ClibPDF - www.fastio.com

Acknowledgements

The authors wish to express their gratitude to the U.S. Department of Transportation for sponsoring the model studies on jointed rock. They also thank Mr. Gregory Baecher, graduate student at M.I.T., for his help in conducting experiments and for reviewing this paper. Part of Mr. Bruhn's contribution was financed by a National Science Foundation Traineeship.

ClibPDF - www.fastio.com

Bibliography

1. Bieniawski, Z.T., Mechanism of Brittle Fracture of Rock, Council for Scientific and Industrial Research, Report MEG 580, Pretoria, South Africa, 1967, 226 pp.

2. Brace, W.F., "Brittle Fracture of Rocks" State of Stress in the Earth's Crust, W.R. Judd, ed., American Elsevier Publishing Co., New York, 1964, pp. 111-178.

3. Bruhn, R.W., The Strength and Deformability of a Model Rock with One Set of Joints Perpendicular to a Principal Stress Axis, MS Thesis, M.I.T., 1969, 220 pp.

4. Byerlee, J.D.,"Frictional Characteristics of Granite under High Confining Pressure," Journal of Geophysical Research, Vol. 72, No. 14, 1967, pp. 3639-3648.

5. Byerlee, J.D., "Brittle-Ductile Transition in Rocks," Journal of Geophysical Research, Vol. 73, No. 14, 1968, pp. 4741-4750.

6. Hayashi, M., "Strength and Dilatancy of Brittle Jointed Mass - The Extreme Value Stochastics and Anisotropic Failure Mechanism," Proc. 1st Cong. Int. Society of Rock Mechanics, Vol. 1, Lisbon, 1967, pp. 295-302.

7. Hoskins, E.R., "The Failure of Thick-Walled Hollow Cylinders of Isotropic Rock," Int. Journal of Rock Mechanics and Mining Sciences, Vol. 6, Pergamon Press, London, 1969, pp.99-125.

8. Jaeger, J.C., "The Frictional Properties of Joints in Rock," Geofisica Pura e Applicata, Vol. 43, Milan, 1959, pp. 148-158.

9. Krsmanovic, D. and Milic, S., "Model Experiments on Pressure Distribution in Some Cases of a Discontinuum," Rock Mechanics and Engineering Geology, Supplementum I, 1964, pp. 72-87.

10. Lane, K.S. and Heck, W.J., "Triaxial Testing for Strength of Rock Joints," 6th Symposium on Rock Mechanics, Univ. of Missouri at Rolla, 1964, pp. 98-108.

11. McClintock, F.A. and Argon, A.S., Mechanical Behavior of Materials, Addison-Wesley Publishing Co., 1966, 770 pp.

12. Maurer, W.C., "Shear Failure of Rock under Compression," Soc. of Petroleum Engineers Journal, 1965, pp. 167-175.

ClibPDF - www.fastio.com

13. Moore, J.F.A., "Experimental Tests on Models of Discontinuous Ground," Proc. 1st Cong. Int. Society of Rock Mechanics, Vol. I, Lisbon, 1967, pp. 307-311.

14. Mueller, L. and Pacher, F., "Modellversuche zur Klaerung der Bruchgefahr gekluefteter Medien," Rock Mechanics and Engineering Geology, Supplementum II, 1965, pp. 7-24.

15. Nelson, R.A., and Hirschfeld, R.C., Modeling a Jointed Rock Mass, M.I.T. Report R68-70, 1968, 218 pp.

16. Orowan, E., "Mechanism of Seismic Faulting;" Rock Deformation, Geological Society of America, Memoir 79, 1966, pp. 323-346.

17. Paterson, M.S., "Experimental Deformation and Faulting in Wombeyan Marble," Bulletin of the Geological Society of America, Vol. 69, 1958, pp. 465-476.

18. Patton, F.D., Multiple Modes of Shear Failure in Rock and Related Materials, Ph.D. Thesis, University of Illinois (University Microfilms, Ann Arbor, Michigan) 1966, 282 pp.

19. Raphael, J.M., Structural Model Investigations for Oroville Dam, Structural and Materials Research, Dept. of Civil Engineering, Series 100, Issue 6, Institute of Engineering Research, Unif. of California, Berkeley, 1960, 164 pp.

20. Rosenblad, L., "Development of a Rock-Like Model Material," Preprint of a paper to be presented at the 10th Symposium on Rock Mechanics at the University of Texas, Austin (Texas), May 1968, 36 pp.

21. Rosengren, K.J. and Jaeger, J.C., "The Mechanical Properties of an Interlocked Low-Porosity Aggregate," Geotechnique, Vol. XVIII, No. 3, 1968, pp. 317-326.

22. Smekal, A.G., "Dynamics of the Brittle Tensile Fracture of Cylindrical Glass Bars," Sitzungsberichte der Oesterreichischen Akademie der Wissenschaften, Vol. 161, 1952, pp. 361-373.

ClibPDF - www.fastio.com

MATERIAL PROPERTIES			π-FACTORS		
Property	Model Material	Rock (granite, quartzite after (1,2))	Factor	Model Material	Rock
ρ Mass density	90 lb/ft^3	~170 lb/ft^3			
σ_c Compressive Strength	3560 psi	34000-72000 psi	$\sigma_c/\rho gD$	35000	9000-19000
			σ_c/σ_t	9	10-17
E Tangent Modulus	1.56×10^6 psi	$5\text{-}10 \times 10^6$ psi	E/σ_c	440	170-300
ν Poisson's Ratio	0.24	0.24	ν	.24	.24
Φ_j *	33°	~35°	Φ_j	33	33

* The joint friction angle was obtained from direct shear tests which will be described in Section C.2.

TABLE I

MATERIAL CHARACTERISTICS OF MODEL MATERIAL AND ROCK

ClibPDF - www.fastio.com

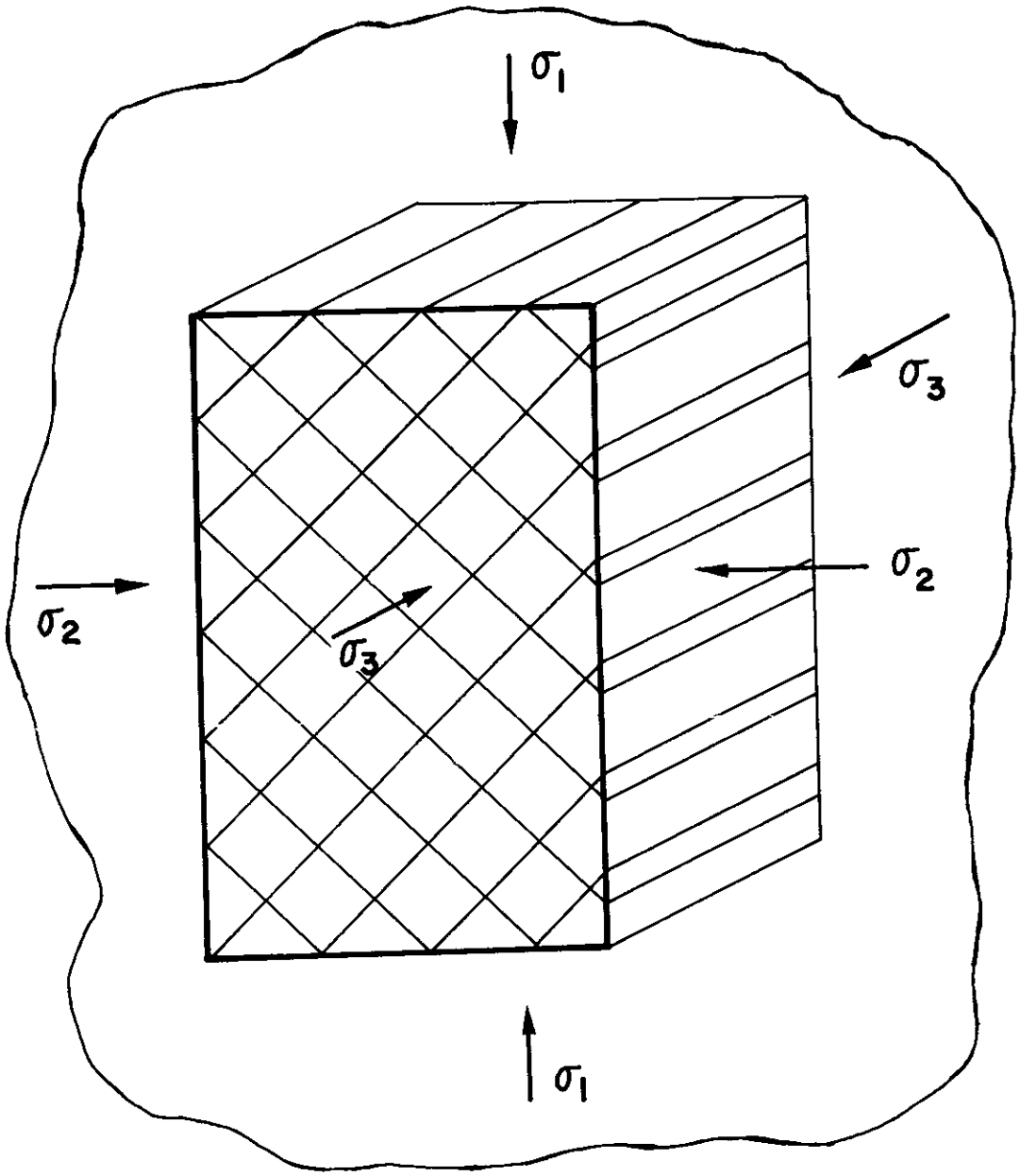

FIG. 1 MODEL OF A ROCK MASS WITH TWO JOINT SETS

ClibPDF - www.fastio.com

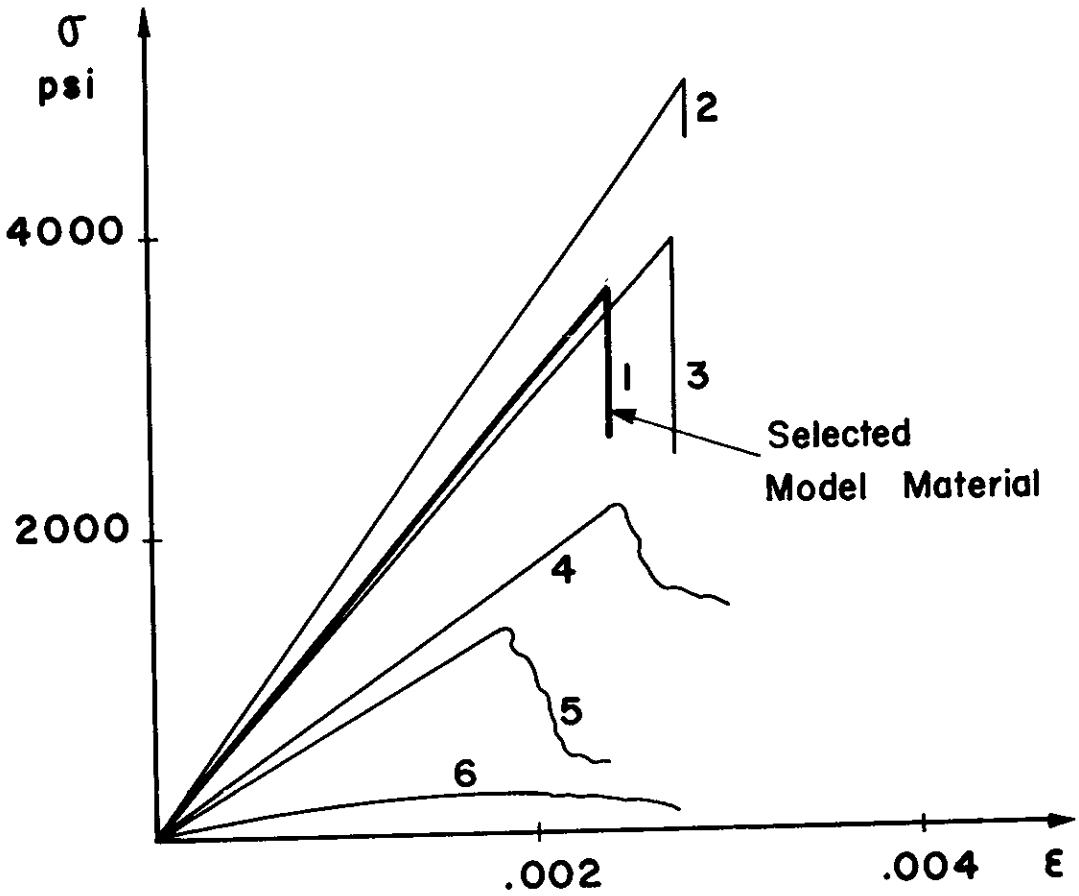

No	GYPSUM TYPE	ADMIXTURE	RATIOS	
			Water / Gypsum	Water / Admixture
1	Hydrocal B II	Celite	.45	32
2	Hydrocal B II	—	.40	
3	Ultracal 60	Celite	.40	16
4	White Molding	—	.65	
5	Hydrocal B II	Sand	.80	.80
6	White Molding	Kaolinite	1.50	3.00

FIG. 2 STRESS-STRAIN CURVES FOR VARIOUS GYPSUM PLASTER MIXES
(Unconfined Compression Tests)

ClibPDF - www.fastio.com

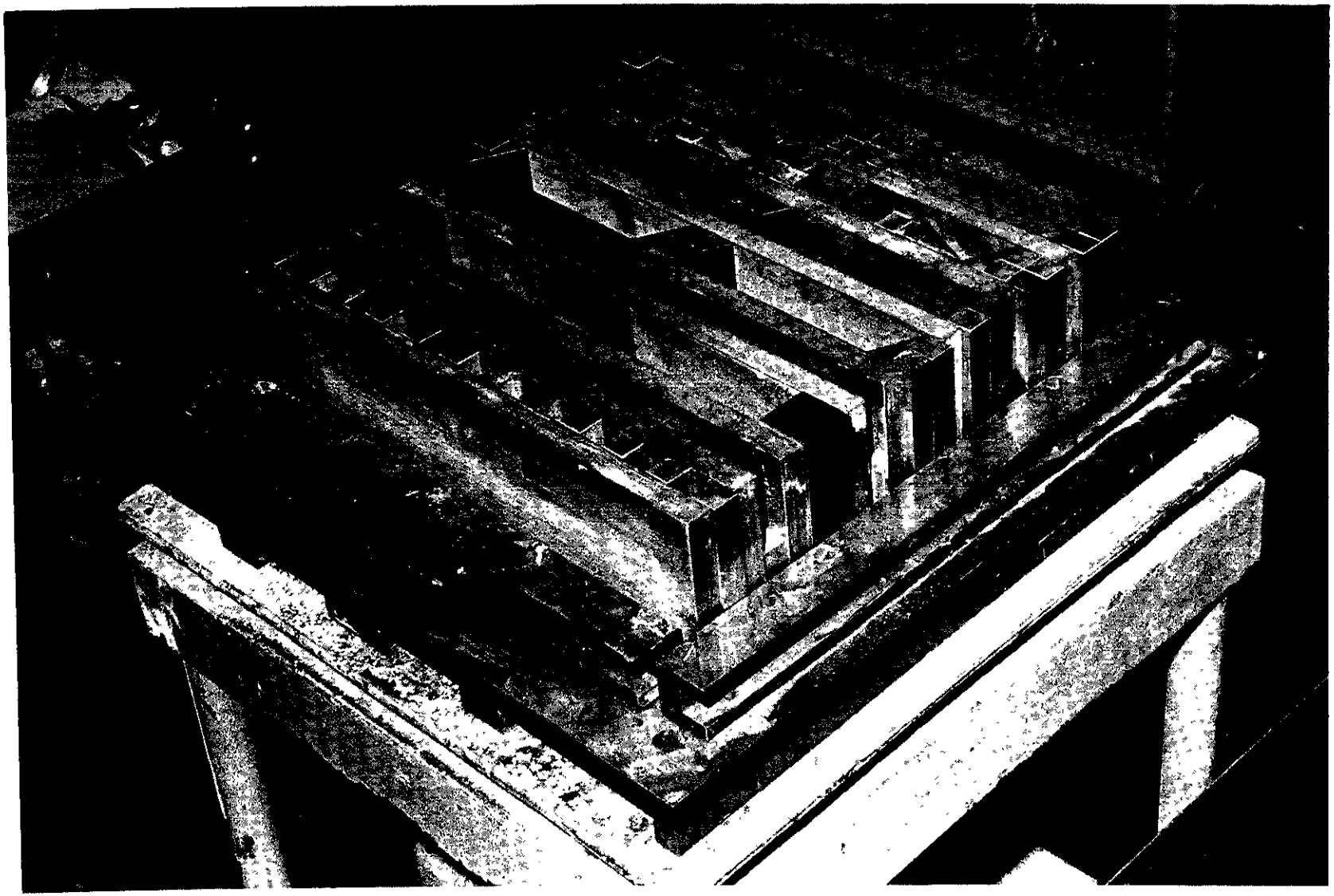

FIG. 3 MOLD

Different Arrangements Are Shown

Clib.PDF - www.fastio.com

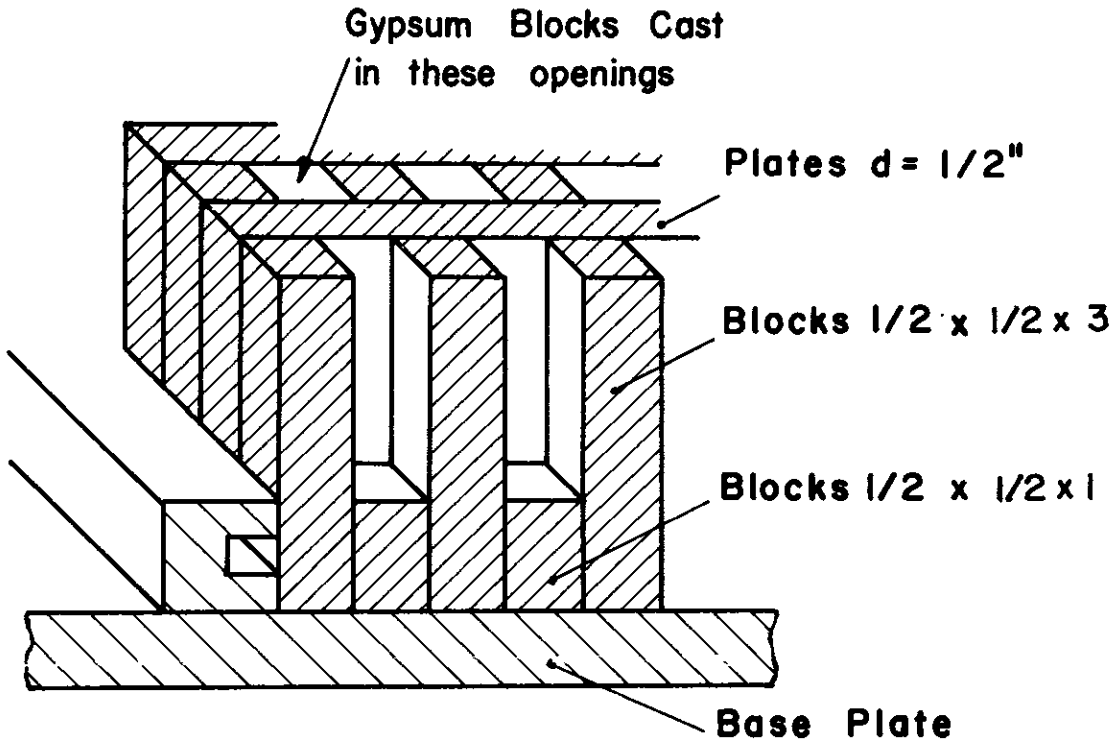

FIG. 4 ISOMETRIC VIEW OF MODEL SET-UP FOR CASTING OF BLOCKS 2" x 1/2" x 1/2"

ClibPDF - www.fastio.com

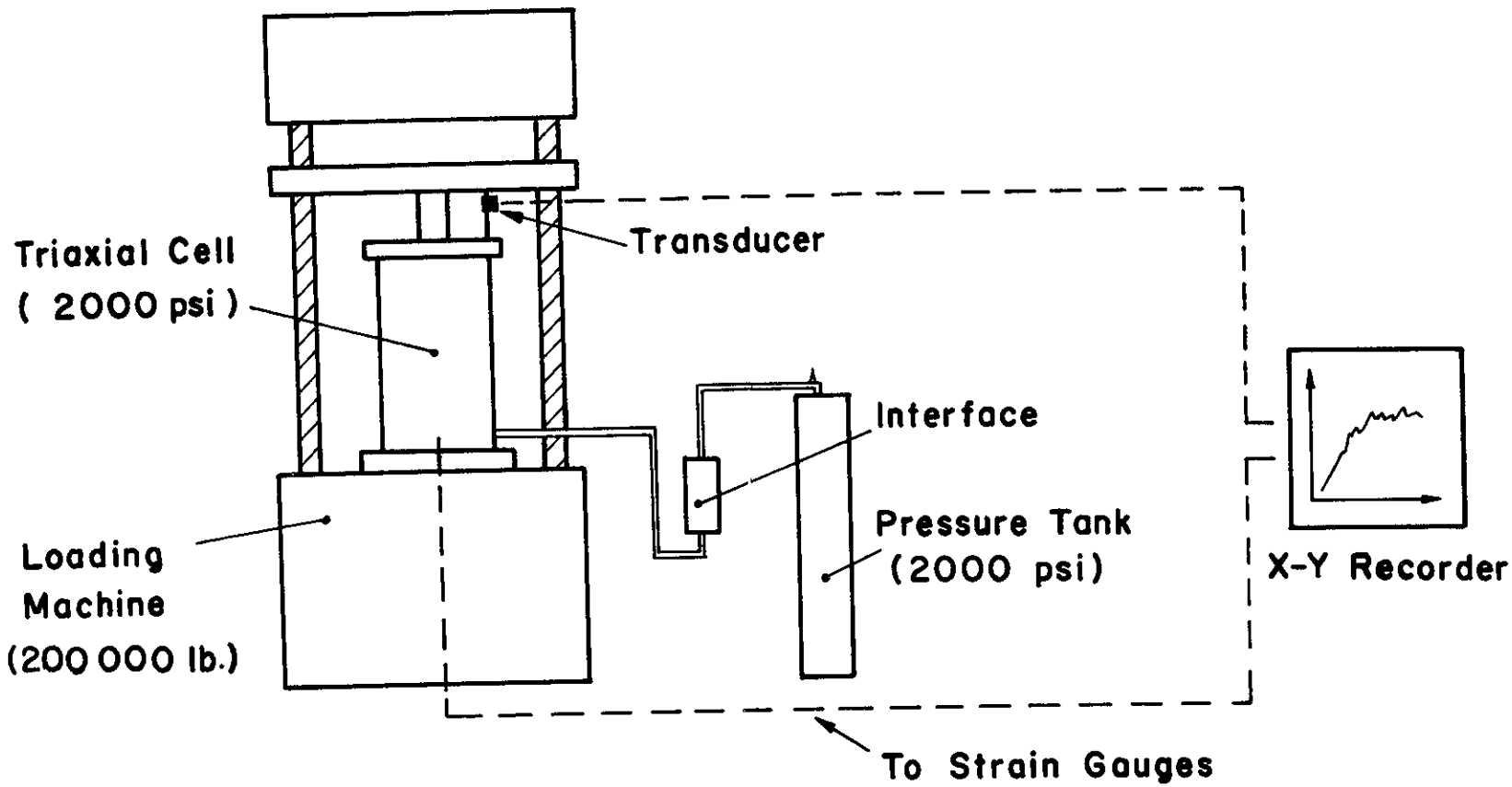

FIG. 5 TRIAXIAL EQUIPMENT

ClibPDF - www.fastio.com

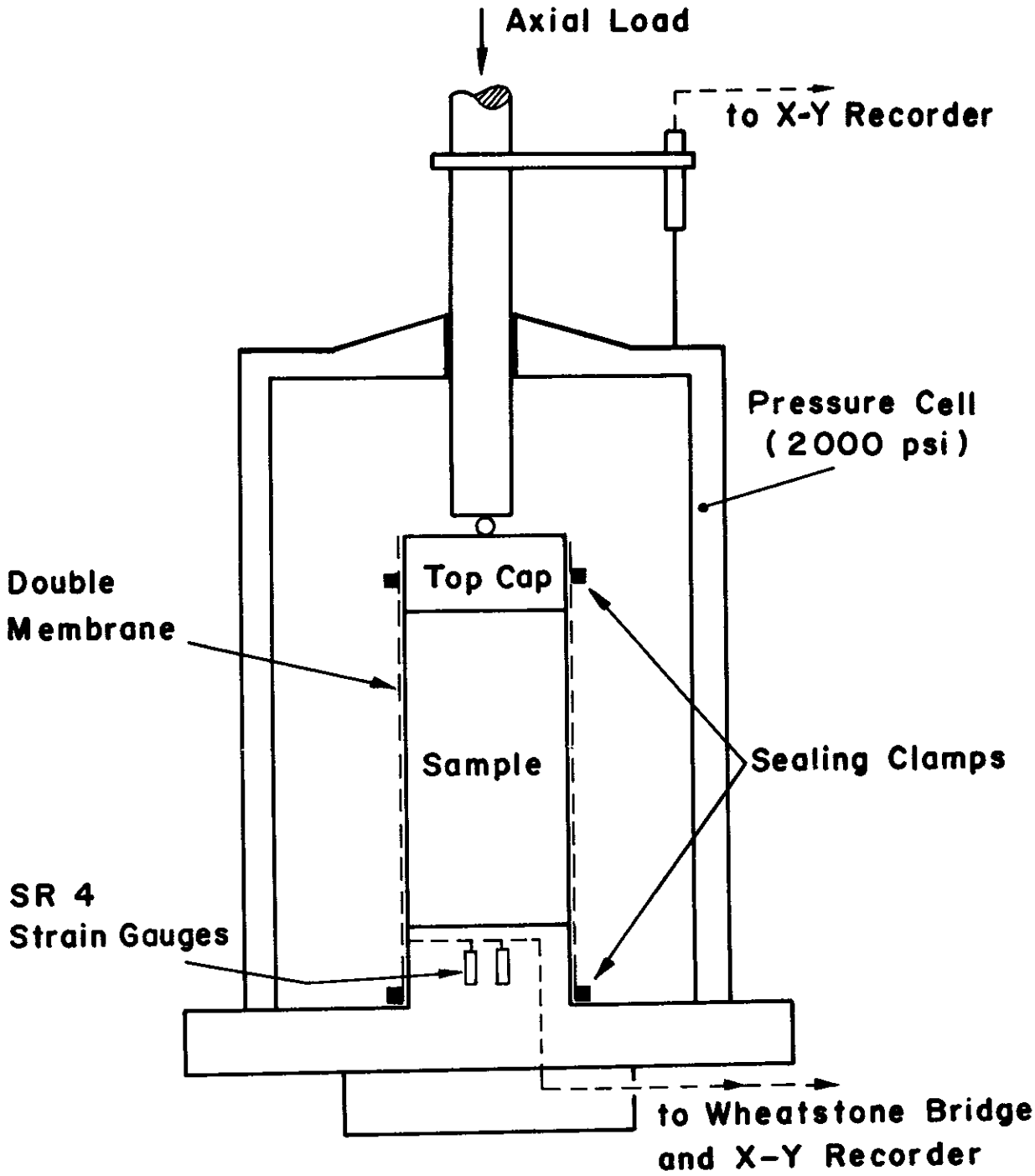

FIG. 6 TRIAXIAL PRESSURE CELL

ClibPDF - www.fastio.com

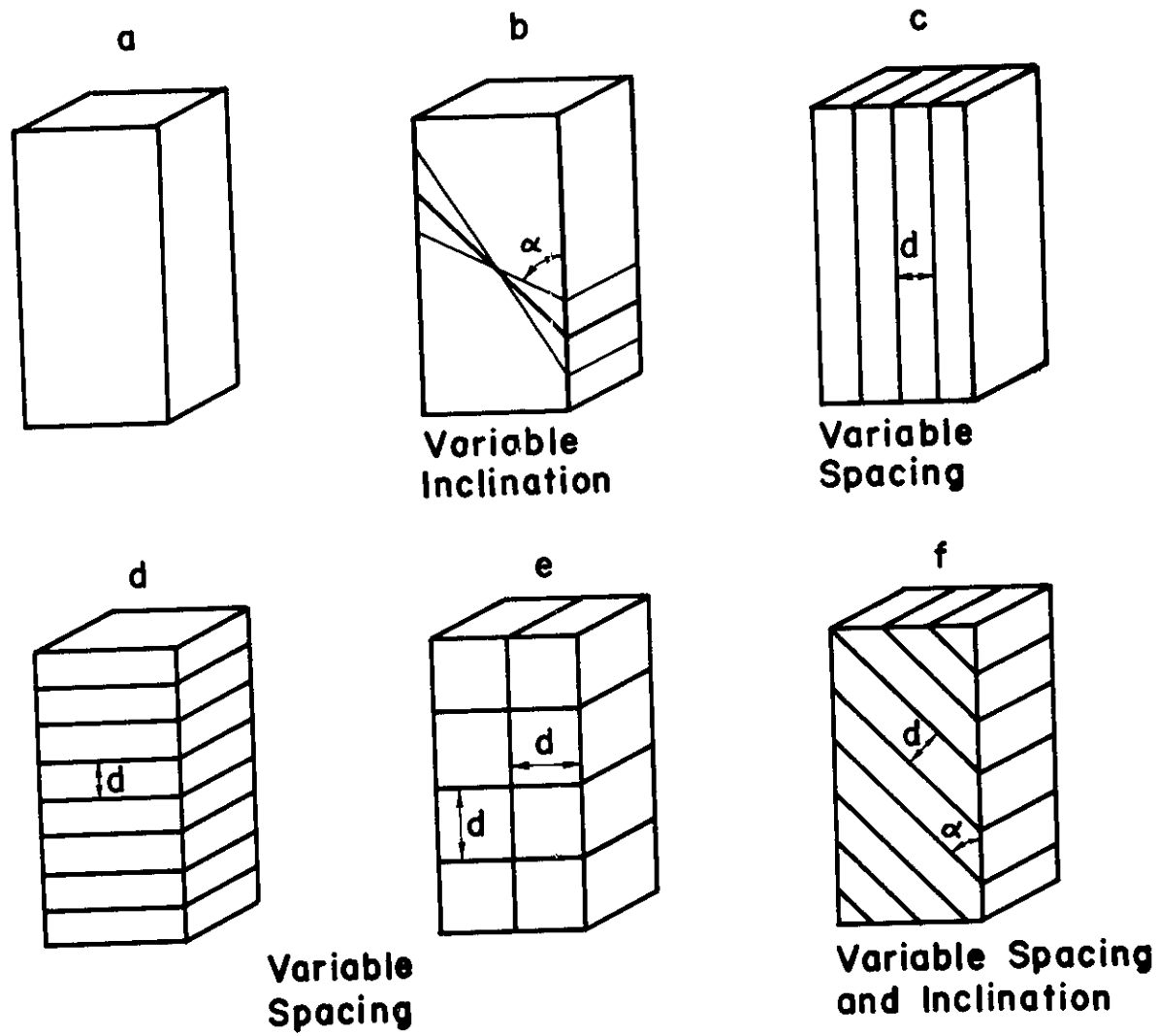

FIG. 7 EXPERIMENTAL SEQUENCE

Each case tested triaxially under different confining stresses

α = 30, 49, 60°
d = 1/2", 1", 2"

Clib PDF - www.fastio.com

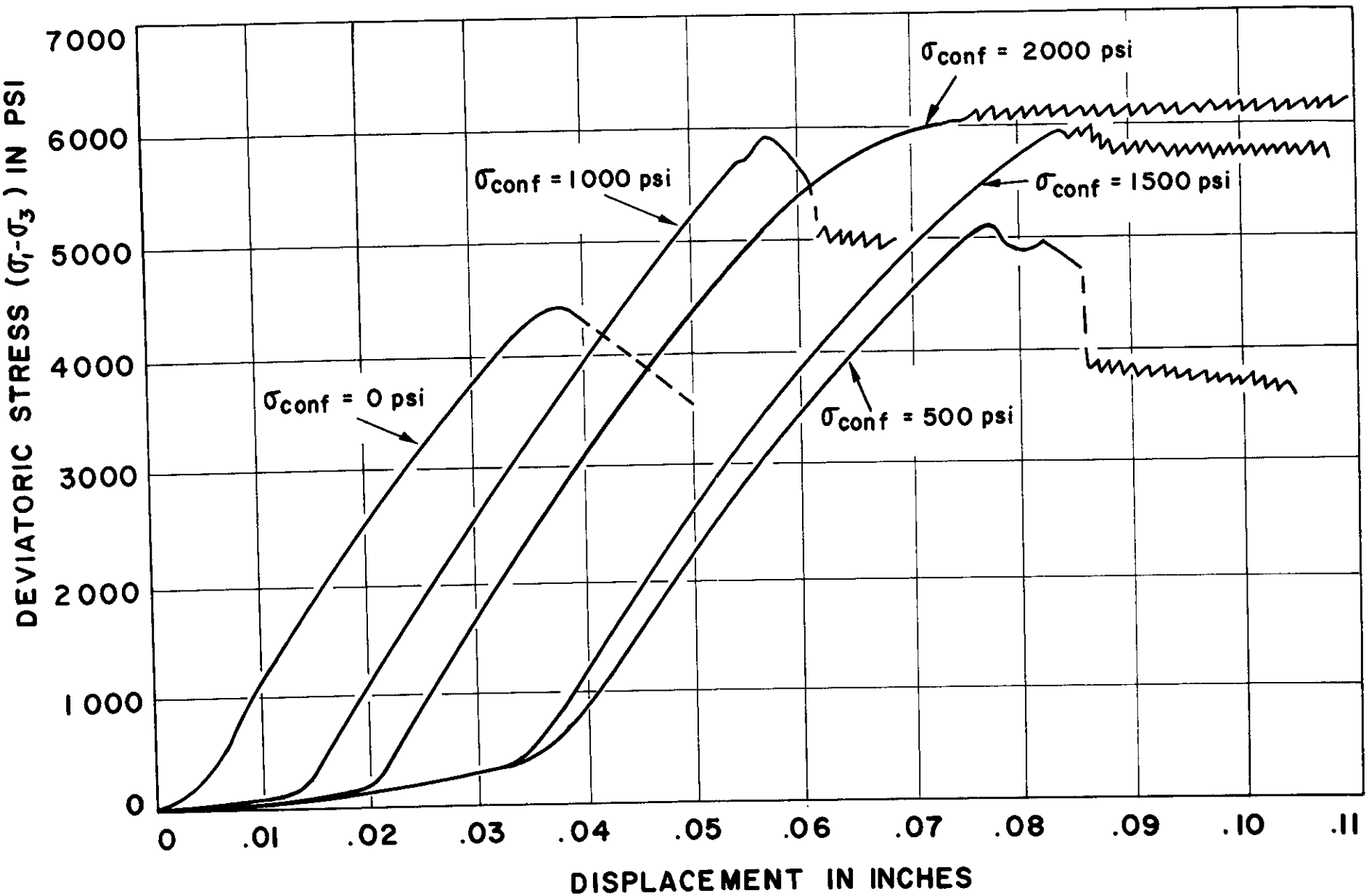

FIG. 8 STRESS-STRAIN CURVES OF INTACT MATERIAL

Clib PDF - www.fastio.com

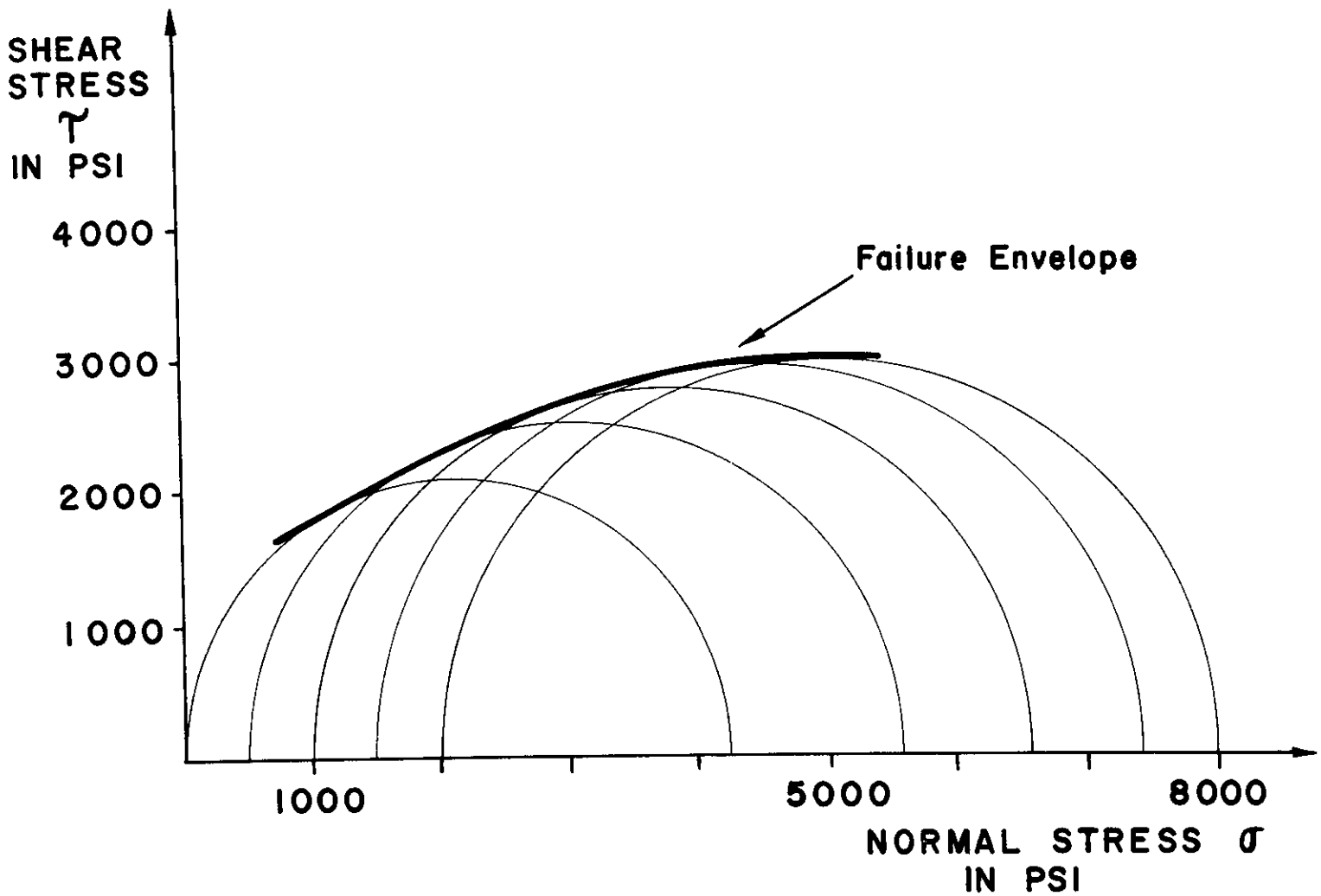

FIG. 9 MOHR DIAGRAM FOR THE INTACT MATERIAL

Clib.PDF - www.fastio.com

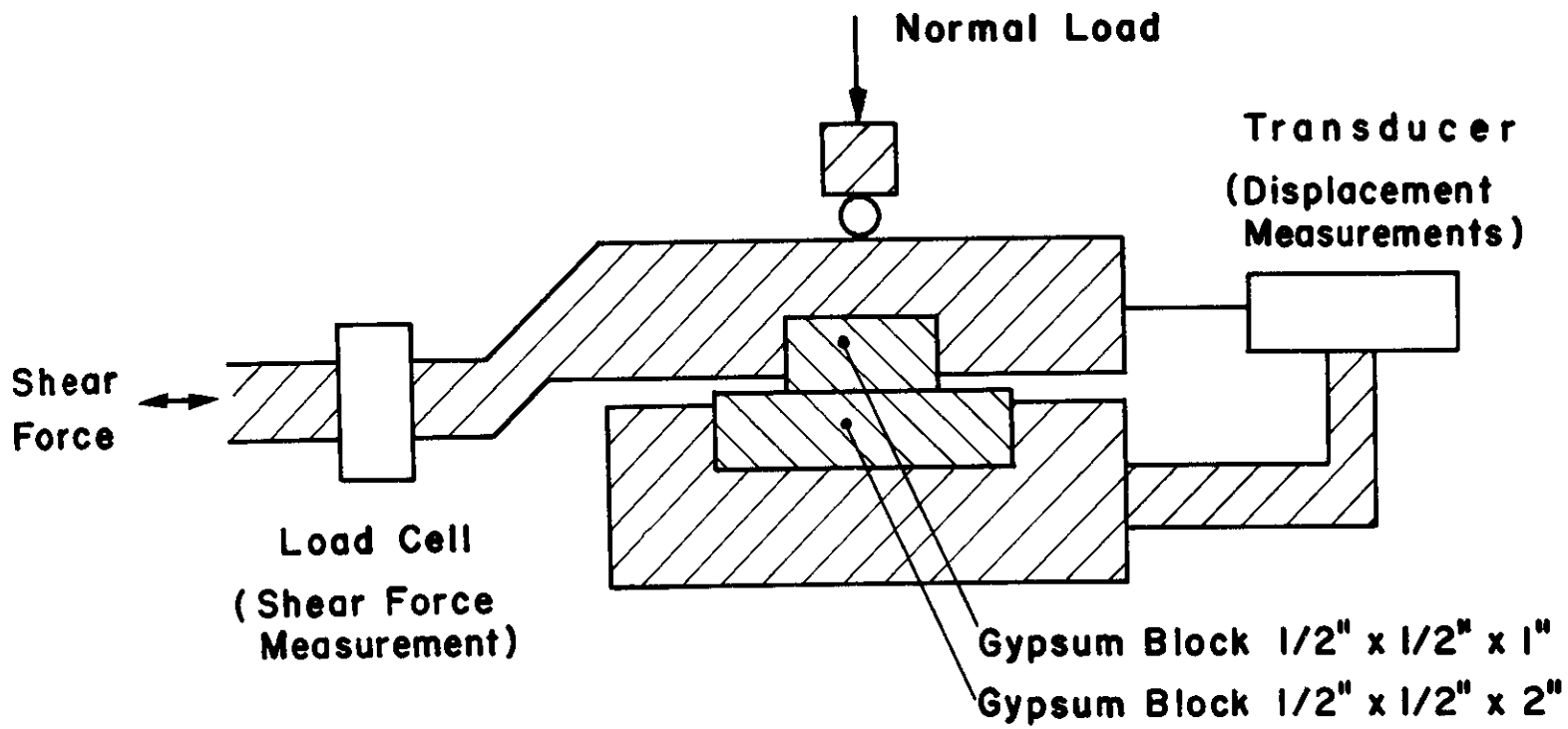

FIG. 10 SCHEME OF DIRECT SHEAR APPARATUS

ClibPDF - www.fastio.com

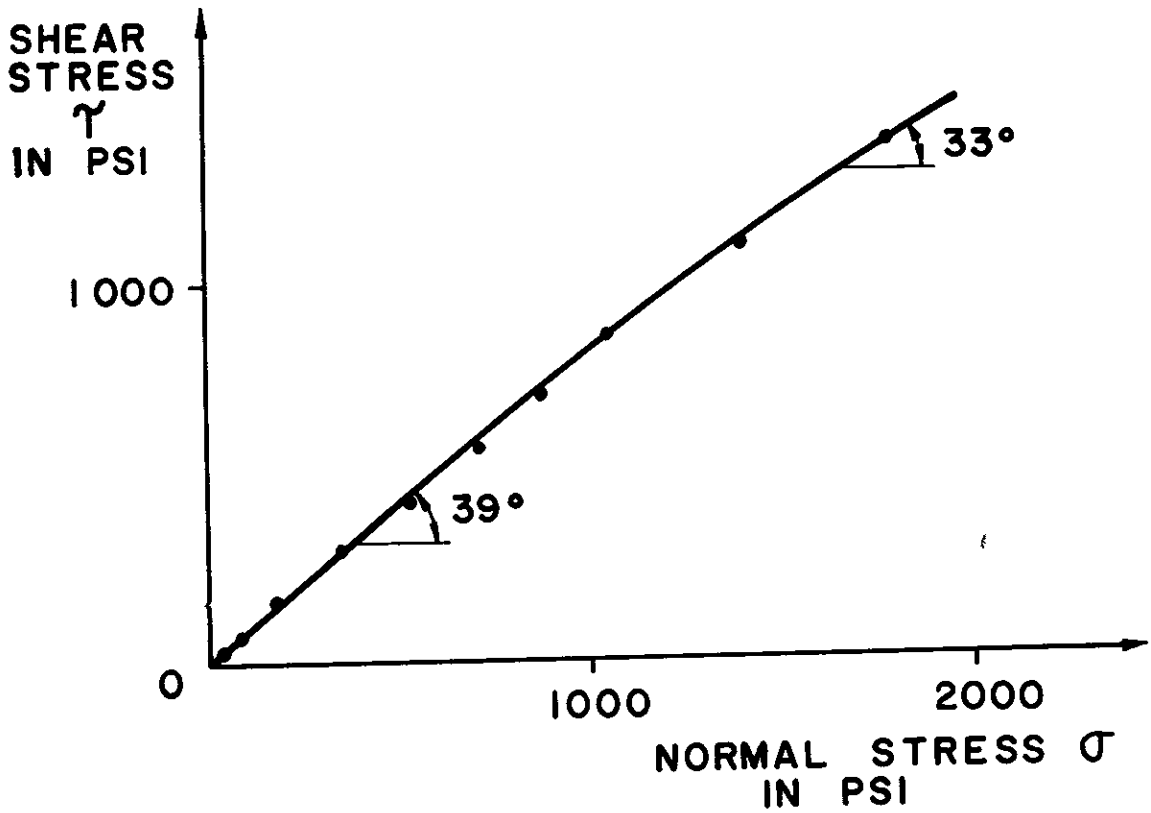

FIG. 11 MOHR ENVELOPE FOR DIRECT SHEAR TEST

ClibPDF - www.fastio.com

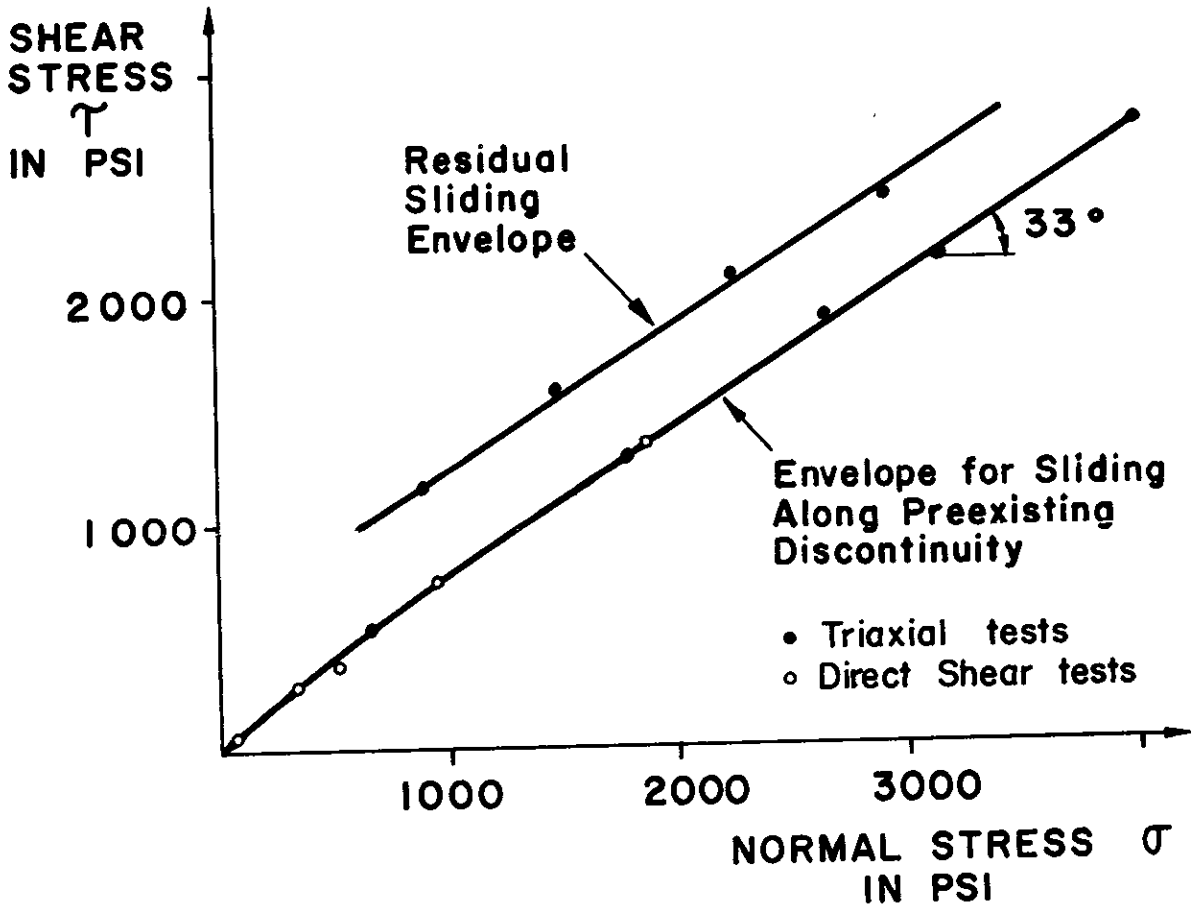

FIG. 12 MOHR ENVELOPES FOR SLIDING IN DIRECT SHEAR AND TRIAXIAL TESTS

ClibPDF - www.fastio.com

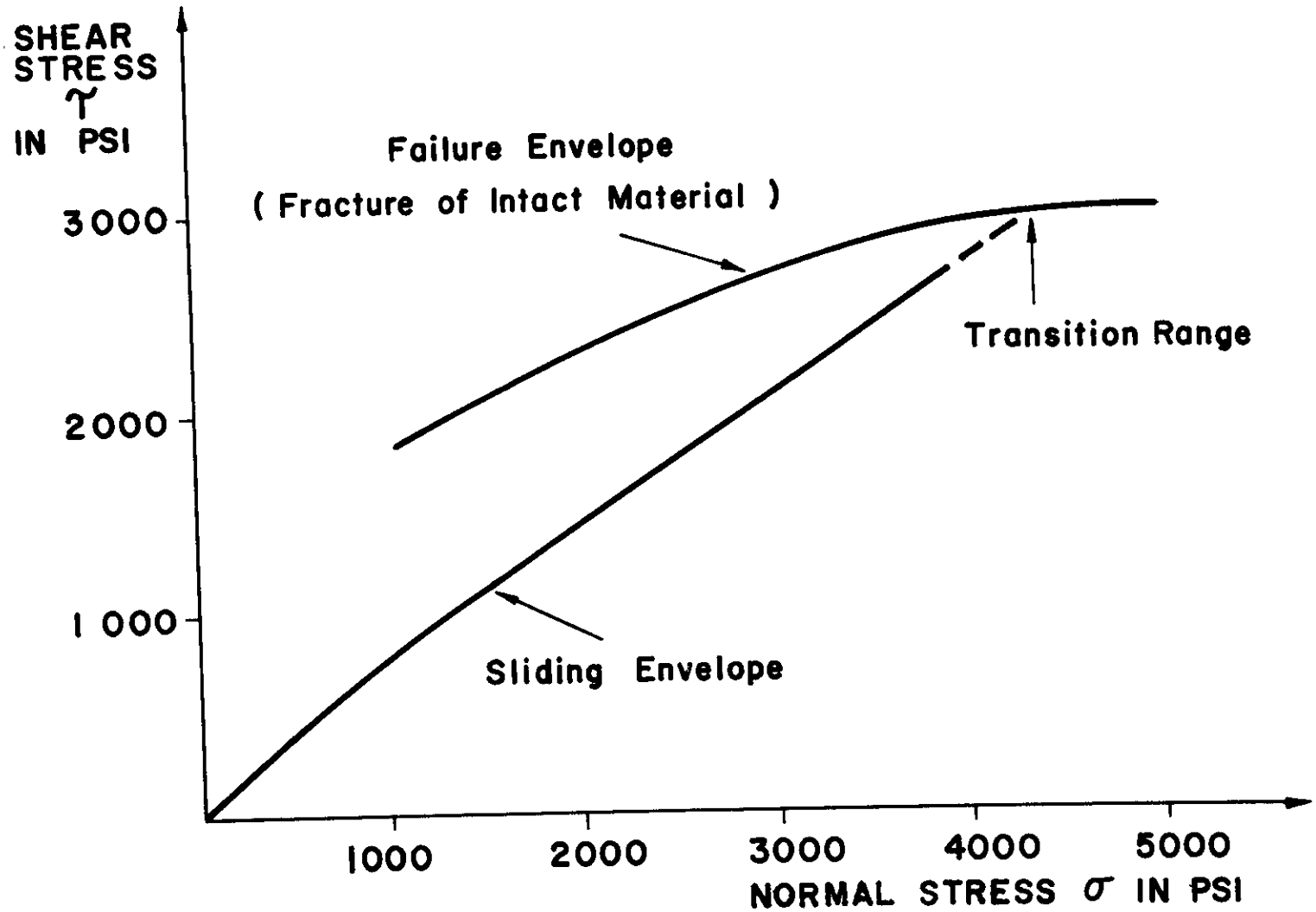

FIG. 13 TRANSITION FROM SLIDING TO FRACTURE

ClibPDF - www.fastio.com

Side view:

Intersection of the Fracture Surfaces with four Joint Planes, Traces Projected into one Plane:

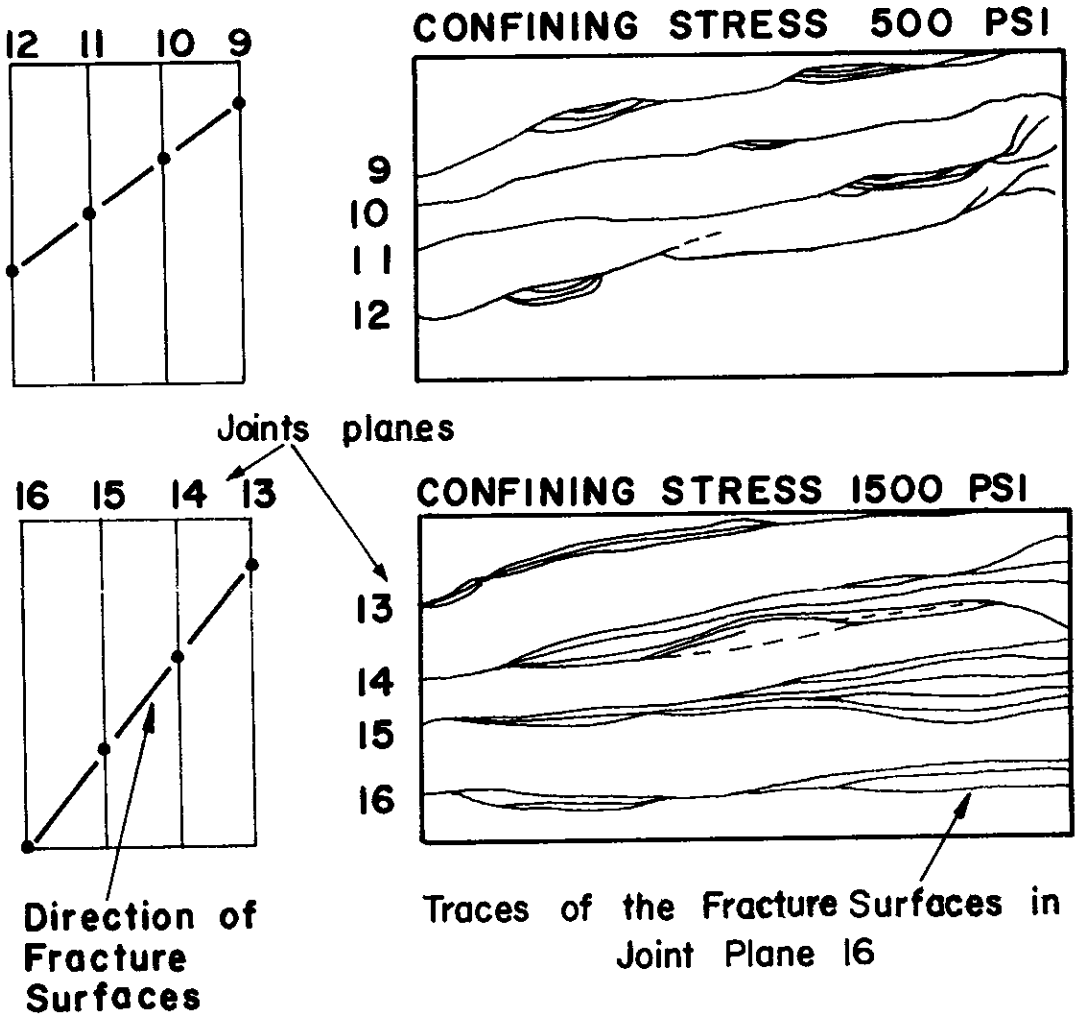

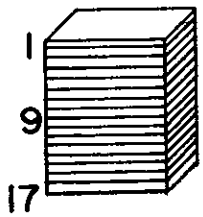

Scheme of Sample and numbering of Joint Planes

FIG. 14 INCREASING NUMBER OF FRACTURE SURFACES WITH INCREASING CONFINING STRESS

(Shown for Samples with Multiple Horizontal Joints, 1/2" Spacing)

ClibPDF - www.fastio.com

VERTICAL JOINTS :

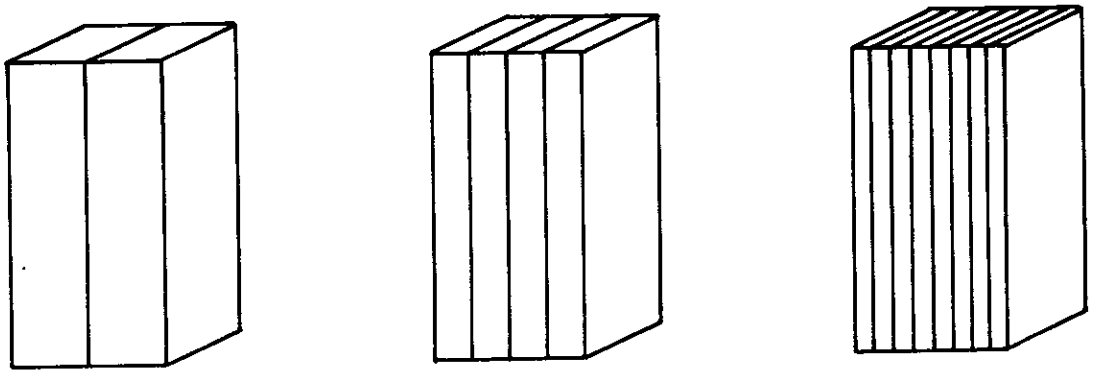

2 Inches

1 Inch

Spacing

1/2 Inch

HORIZONTAL JOINTS :

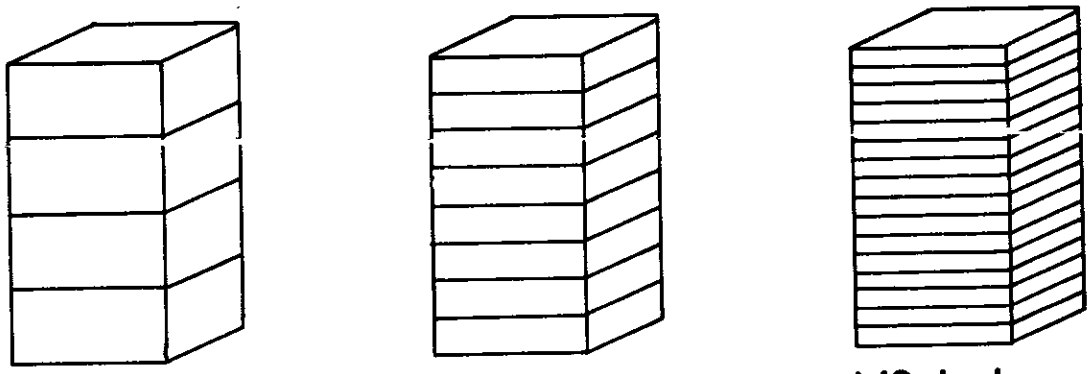

2 Inches

1 Inch

Spacing

1/2 Inch

ORTHOGONAL JOINTS :

1/2 Inch Spacing

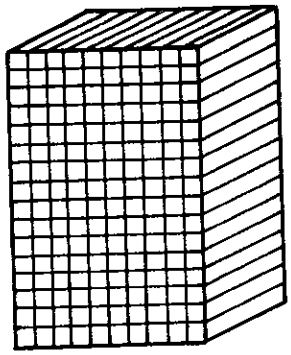

FIG. 15 JOINT CONFIGURATIONS

ClibPDF - www.fastio.com

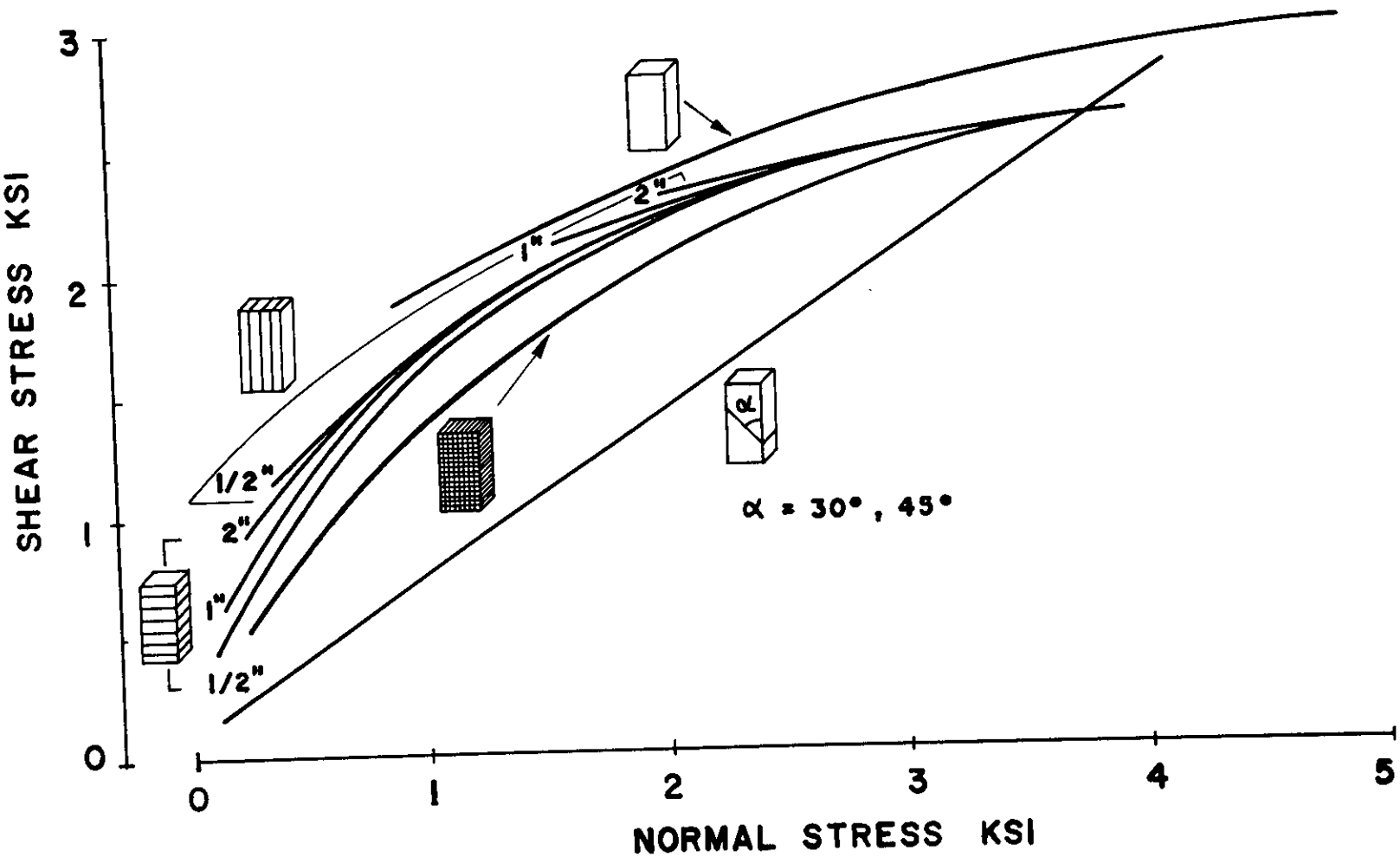

FIG. 16 MOHR ENVELOPES FOR INTACT AND JOINTED GYPSUM MODELS

Click PDF - www.fastio.com

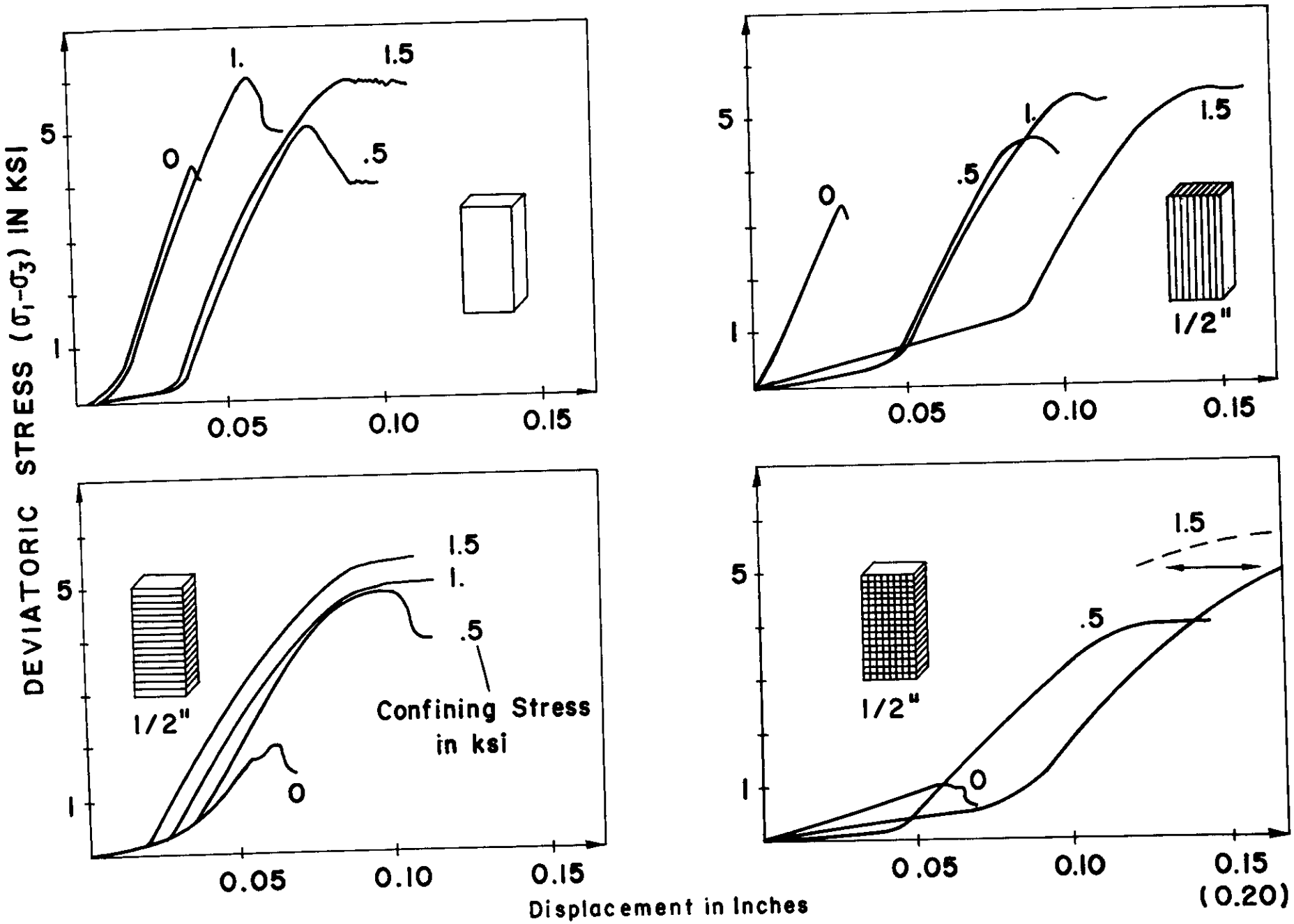

FIG. 17 STRESS-DISPLACEMENT CURVES

For Different Joint Configuration and Confining Stresses

ClibPDF - www.fastio.com

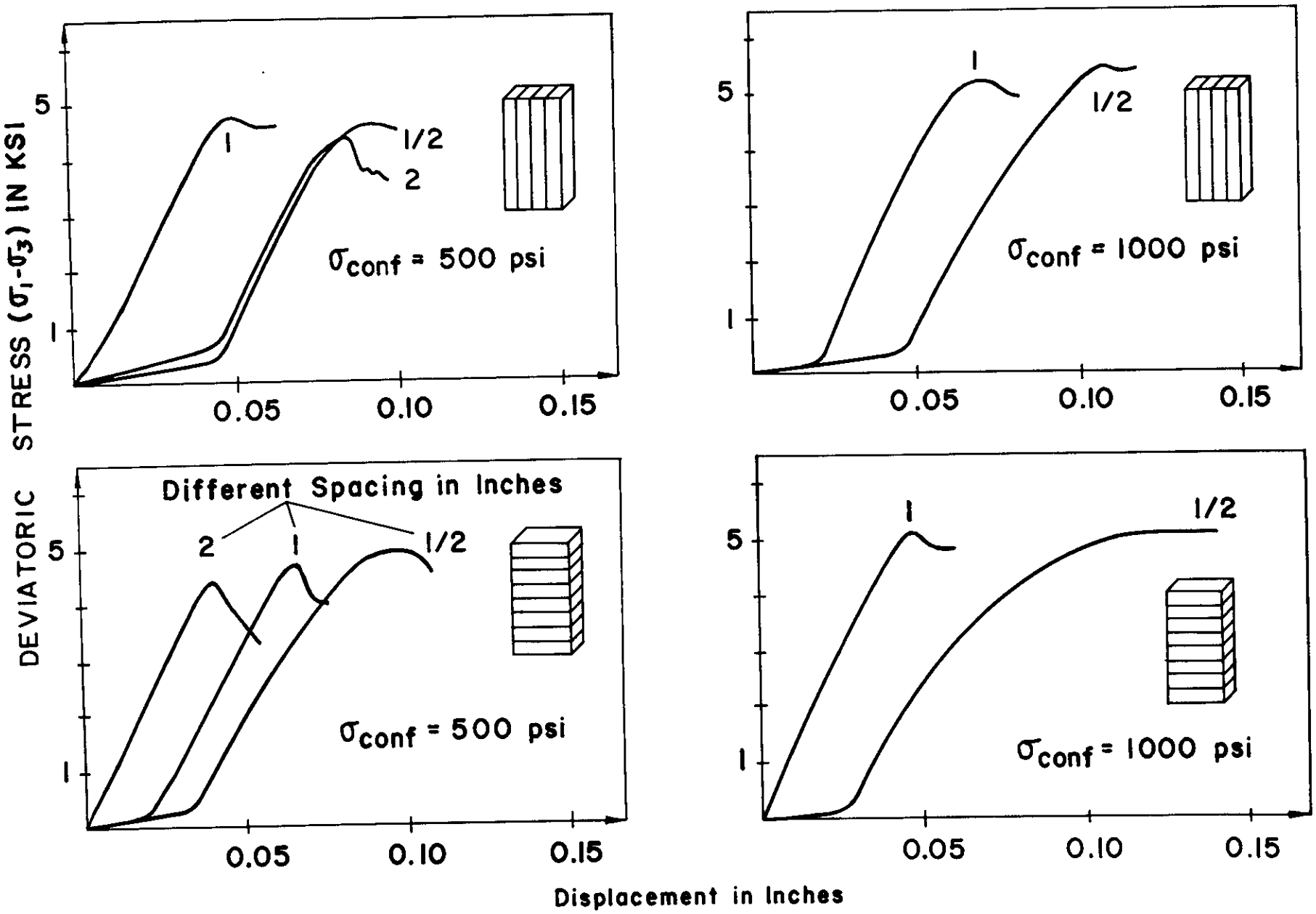

FIG. 18 STRESS - DISPLACEMENT CURVES

For Different Joint Spacings and Confining Stresses

Guide PDF - www.fastio.com

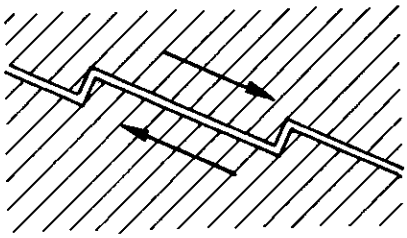

Observed "Steps" on Failure Surface
and Direction of Movement

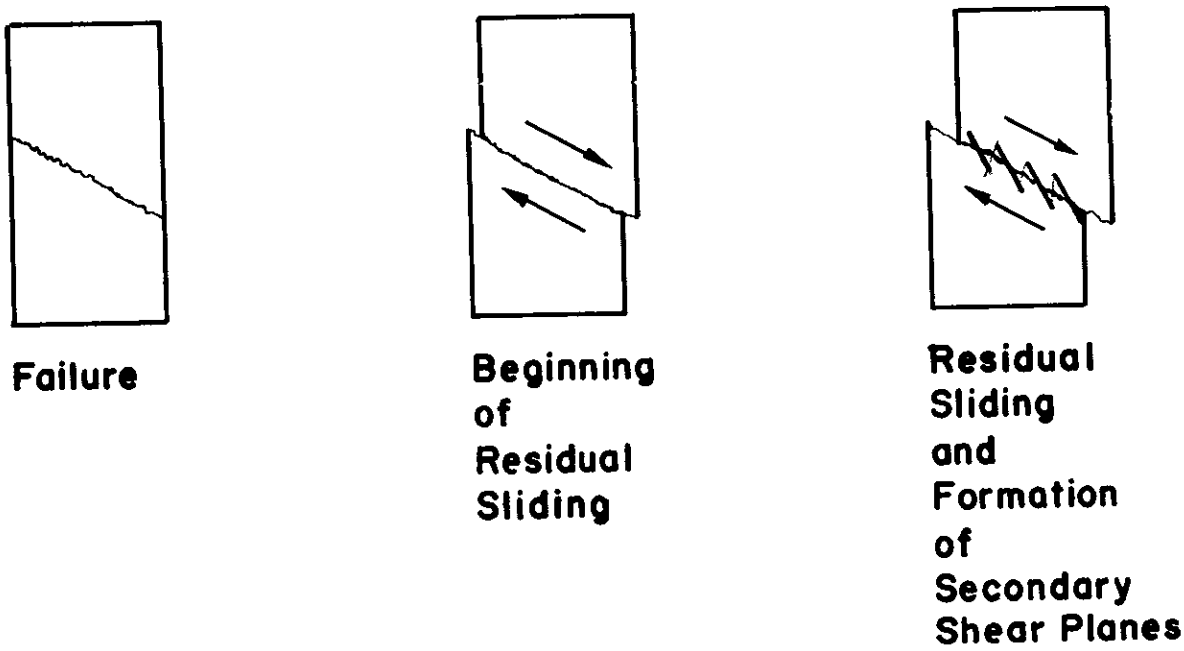

POSSIBLE MECHANISM LEADING TO "STEPS"

FIG. 19 SLICKENSIDE FEATURES ON FAILURE SURFACE

ClibPDF - www.fastio.com